Marine and Petroleum Geology 170 (2024) 107115

Contents lists available at ScienceDirect

Marine and Petroleum Geology

journal homepage: www.elsevier.com/locate/marpetgeo

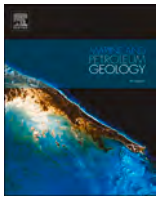

Pervasive calcite veins and cleavage dilation in low-grade metamorphic rocks as a marker of lower Jurassic rift-basin margins: A signature of microbial colonization

S. Fabbi [a,*], M. Borrelli [b], G. Innamorati [a], L. Aldega [a], M. Daëron [c], E. Perri [b], M. Santantonio [a]

[a] Dipartimento di Scienze della Terra, Sapienza Università di Roma, Piazzale Aldo Moro 5, 00185, Rome, Italy
[b] Dipartimento di Biologia, Ecologia e Scienze Della Terra, Università Della Calabria, Via Pietro Bucci, 87036, Arcavacata di Rende, Cosenza, Italy
[c] Laboratoire des Sciences du Climat et de l'Environnement, LSCE/IPSL, CEA-CNRS-UVSQ, Université Paris-Saclay, Orme des Merisiers, 91191, Gif-sur-Yvette, France

A B S T R A C T

We report herein for the first time the occurrence of low-grade metamorphic rocks dilated by the growth of calcite veins induced by microbial communities inhabiting the cleavage planes. This process took place at the rock/sea-water interface in a rocky shore environment when the Hercynian basement rocks of the European-Iberian continental margin in Calabria (Italy) experienced stepwise flooding by a shallow tropical sea in the Early Jurassic, a process which was accompanied by synsedimentary extension, resulting in the birth of the Longobucco Basin. The veins exhibit a multiphase filling history, as, in an early phase, microstromatolites lining the walls of cleavage planes document the initial development of microbial biofilms. Subsequently, the growth of bands of radiaxial fibrous calcite enlarged the cavities through force of crystallization, also producing fissures at a high angle with respect to cleavage, which were in turn enlarged by crystal growth. Carbonate clumped isotope analysis indicates crystallization of calcite from sea water, at temperatures (T_{47}) ranging from *c.* 33 to *c.* 44 °C. The inferred palaeoenvironment is that of a rocky coastline, locally with tide pools, where the seawater lapped cliffs made of Palaeozoic metasandstone. Microbially induced mineralization was a very rapid process, as clasts of veined metamorphic rocks are found in only slightly younger Early Jurassic deposits, like the sub-reefal carbonate bodies that grew in the Pliensbachian attached to the Palaeozoic bedrock. The occurrence of low-grade metamorphic rocks bearing calcite veins can be mapped in the field for kilometers, following the high-angle unconformity that separates the shallow-water carbonates from the basement. This microbial overprint therefore is a marker of the margins of a rift basin, where the exposure of basement rock along steep submarine surfaces was the result of footwall unroofing.

1. Introduction

Microbially induced calcium carbonate precipitation is a well-known process (e.g., Burne and Moore, 1987; Riding, 2002; Konhauser and Riding, 2012), and is commonly related to the metabolic activities and/or biochemical properties of bacteria, algae, fungi, and even viruses (Bontognali et al., 2008; Petrash et al., 2017 Perri et al., 2017, 2022). The deposits originated by this process are known as "microbialites" (Burne and Moore, 1987; Riding, 2000) which are commonly characterized by an array of (bio-) sedimentary features, such as clotted fabrics, micropeloidal textures, cementstones, stromatolites, and polymetallic crusts in general (Reitner, 1993; Riding, 1991; Sano and Nakashima, 1997; Dupraz and Strasser, 1999; Webb et al., 1998; Préat et al., 2011; Reolid and Abad, 2019; Qin et al., 2020). Microbialites can form over a wide range of environmental conditions: from hypersaline to fresh-water alkaline waters (e.g., Last et al., 2010; Perri et al., 2019, 2024; Borrelli et al., 2019, 2021), in both photic and aphotic settings, including the so-called "cryptic" environments, like caves, macro and microcavities, fissures and pores of rocks and sediments (e.g. Zankl, 1993; Sanfilippo et al., 2015; Melim et al., 2016; Borrelli et al., 2024). Studies on microbial carbonates in cryptic environments refer to endostromatolites (Monty, 1982) or to endolithic microbialites, growing within empty cavities in tropical reef frameworks (e.g., Monty, 1982; Reitner, 1993), in mid-latitude shallow-marine bioconstructions (Bernasconi et al., 2015), or in various continental cold-climate environments (Lacelle, 2007), documented both in the modern and fossil record. Non-carbonate microbialites such as *Frutexites* or *Frutexites*-like structures are commonly considered markers of cryptic environments, being produced by cryptobiontic communities colonizing the walls of submarine cavities and fractures (Walter and Awramik, 1979; Myrow and Coniglio, 1991; Rodríguez-Martínez et al., 2011; Heim et al., 2017; Neubeck et al., 2021; Champenois et al., 2023).

In the Longobucco Basin (northern Calabria, Italy), at the contact between the Paleozoic basement and Pliensbachian photozoan carbonates, the presence of puzzling calcite veins and associated mineralizations can be observed along cleavage planes and fractures in phyllites

* Corresponding author.
E-mail address: simone.fabbi@uniroma1.it (S. Fabbi).

https://doi.org/10.1016/j.marpetgeo.2024.107115
Received 10 July 2024; Received in revised form 28 August 2024; Accepted 14 September 2024
Available online 19 September 2024

and metasandstones (Caloveto Group; Santantonio and Teale, 1987). Bouillin and Bellomo (1990) noticed the dilation of low-grade metamorphic rocks (their "swollen phyllites") and growth of calcite bands in one remarkable outcrop, an observation which was subsequently duplicated in several key localities (Fig. 1) throughout the Longobucco Basin during a geological mapping project in the region (Santantonio et al., 2016; Innamorati and Santantonio, 2018; Santantonio and Fabbi, 2020; Innamorati et al., 2024). Notably, calcite veins mark metamorphic basement/limestone contacts representing preserved basin-margin onlaps, having a lateral continuity of several kilometres.

In this paper, we describe the origin of calcite veins in low-grade metamorphic rocks through sedimentology, micropaleontology, petrography, and chemical, SEM, standard C and O isotopes characterization and also clumped isotopes analysis. We interpret their origin as the product of the mineralization of microbial communities colonizing cleavage planes during the initial stages of flooding of a Hercynian mainland by Tethyan sea waters. Finally, we discuss the regional occurrence of dilated low-grade metamorphic rocks, and their predictive potential in basin analysis as an unexpected tool for outlining the boundaries of a severely deformed Jurassic rift basin.

2. Geological setting

The Longobucco Basin (Fig. 1) in Sila Greca (northern Calabria, Italy) hosts a >1.5 km thick stratigraphic succession, starting with Rhaetian continental red-beds and followed by mixed carbonate/siliciclastic shelf deposits, resting on the Hercynian basement (granitoids and low-to very low-grade metamorphic rocks; Langone et al., 2010, and references therein). Rift-related synsedimentary extension in the Early Jurassic, with two main pulses occurring at the Sinemurian/Pliensbachian boundary and in the Toarcian, produced the accommodation space for a deep marine carbonate/siliciclastic succession ranging into the Early Cretaceous (Longobucco Group). Both tectonic phases are associated with a network of neptunian dykes cutting the basement (Young et al., 1986; Bouillin and Bellomo, 1990; Santantonio et al., 2016). A coeval thinner succession (Caloveto Group), starting in the Pliensbachian, is instead observed on and around intrabasinal structural highs and at rift shoulders, with shallow-water benthic carbonate factories colonizing the basin-facing margins of footwall blocks in the form of fringing carbonate bodies (Innamorati and Santantonio, 2018; Santantonio and Fabbi, 2020).

3. Methods

Rock samples were analyzed through standard (30 μm-thick) thin sections examined by transmitted light optical microscopy. Selected thin sections and fresh broken samples were carbon coated and further analyzed through a Scanning Electron Microscope (SEM) at Università della Calabria with a ZEISS Crossbeam 350, operating in a range of 5–20 kV with a working distance between 6 mm and 15 mm and equipped with an EDS EDAX OCTANE Elite Plus, that permitted to obtain EDS point spectra and elemental maps. Additional micro-Raman spectrometry was performed on selected thin sections using a Jasco NRS-5100 spectrometer equipped with a 532 nm laser wavelength filter (0.3 mW, 100× objective).

Six calcite vein samples from the metamorphic rocks/limestone boundary of the Longobucco Basin were powdered for C, O, and clumped isotopes analyses. Carbonate samples were converted to CO_2 by phosphoric acid reaction at 90 °C in a common, stirred acid bath for 30 min. Initial phosphoric acid concentration was 103% (1.91 g/cm^3) and each batch of acid was used for 7 days. After cryogenic removal of water, the evolved CO_2 was helium-flushed at 25 mL/mn through a purification column packed with Porapak Q (50/80 mesh, 1 m length, 2.1 mm ID) and held at −20 °C, then quantitatively recollected by cryogenic trapping and transferred into an Isoprime 100 dual-inlet mass spectrometer equipped with 6 F collectors (m/z 44–49). Each analysis took about 2.5 h, during which analyte gas and working reference gas were allowed to flow from matching, 10 mL reservoirs into the source through deactivated fused silica capillaries (65 cm length, 110 μm ID). Every 20 min, gas pressures were adjusted to achieve m/z = 44 ion beam current of 80 nA, with differences between analyte gas and working gas generally below 0.1 nA. Pressure-dependent background current corrections were measured 12 times for each analysis. All background measurements from a given session within ±6 h of any given analysis were used to determine a mass-specific relationship for that analysis, linking background ion current (Z_m), total m/z = 44 current (I_{44}), and time (t): $Z_m = a\ I_{44} + P(t)$, with P being a polynomial of degree 2 to 4. Background-corrected ion current ratios (δ_{45} to δ_{49}) were converted to $\delta^{13}C$, $\delta^{18}O$, and "raw" Δ_{47} values as described by Daëron et al. (2016) using the IUPAC oxygen-17 correction parameters (Brand et al., 2010). The isotopic composition ($\delta^{13}C$, $\delta^{18}O$) of our working reference gas was computed based on the nominal isotopic composition of all ETH carbonate standards (Bernasconi et al., 2018) and an oxygen-18 acid fractionation factor of 1.00813 (Kim et al., 2007). Raw Δ_{47} values were then converted to the I-CDES reference frame (Bernasconi et al., 2021) using a pooled regression approach (Daëron, 2021) as implemented by the D47crunch Python library. Full analytical errors are derived from the external reproducibility of unknowns and standards (N_f = 37) and conservatively account for the uncertainties in raw Δ_{47} measurements as well as those associated with the conversion to the I-CDES reference frame (Daëron, 2021). Crystallization temperatures were estimated from Δ_{47} based on the OGLS23 composite calibration (Daëron and Vermeesch, 2024).

4. Results

4.1. Metamorphic basement of the Longobucco basin

The most instructive exposure of calcite veins in the low-grade metamorphic rocks is found along the SP 251 road, connecting the remote villages of Caloveto and Bocchigliero in Northern Calabria, near the km 9 roadsign (Fig. 2A). Here, the low-grade metamorphic rocks are pervasively dilated by calcite veins. Most veins mark cleavage planes, which are locally sub-horizontal, but other veins are oblique to sub-orthogonal with respect to cleavage (Fig. 2D and E). The rock volume affected by this dilation is limited as the veins disappear a few tens of cm away from the paleosurface representing the basement/carbonates unconformity. Moreover, the low-grade metamorphic rocks are dismembered by several sets of neptunian dykes, ascribable to two different phases of fracturing. The first generation of neptunian dykes is made up of typical shallow-water carbonate sediments (Fig. 2C) and can be ascribed to the early Pliensbachian based on the known age of the Lower Caloveto Fm. To which they are attributed (Santantonio and Fabbi, 2020). The second generation is instead represented by Toarcian red pelagic mudstone/wackestone dykes cutting both the Paleozoic basement, and locally running along cleavage planes, and the first generation of neptunian dykes (Fig. 2C, D, G). Dark cm-thick *Frutexites*-like structures occur either along the basement rocks/limestone unconformity or within neptunian dykes (Fig. 2E).

4.2. The calcite veins

Calcite veins fill sheet cracks following cleavage planes in the metasandstones (Fig. 3A and B). Cleavage-parallel calcite veins span from ~0.1 to ~10 mm in width, commonly showing an internal structure characterized by two main carbonate microfacies: stromatolitic crusts and large radiaxial-fibrous calcite crystals bands:

- Stromatolitic crusts are characterized by the accretion of multiple generations of dark micritic laminae commonly showing a dominant flat to undulated fabric, alternated with peloidal laminae (Fig. 3B and C), accounting for a thickness ranging from 2.4 to 5.6 mm.

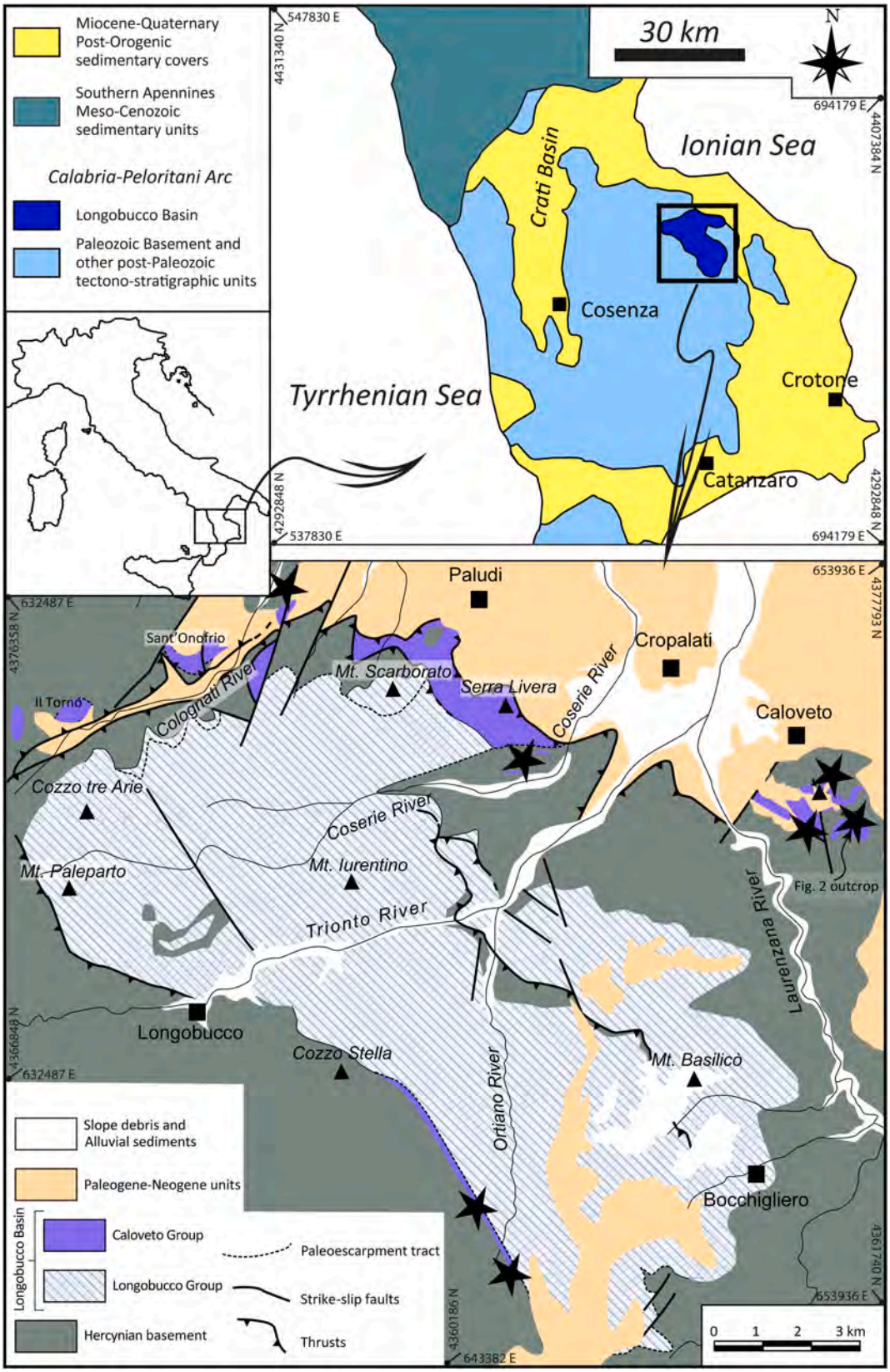

Fig. 1. – Location and geological setting of the Longobucco Basin (modified after Santantonio and Fabbi, 2020). Black stars are occurrences of metamorphic rocks with calcite veins.

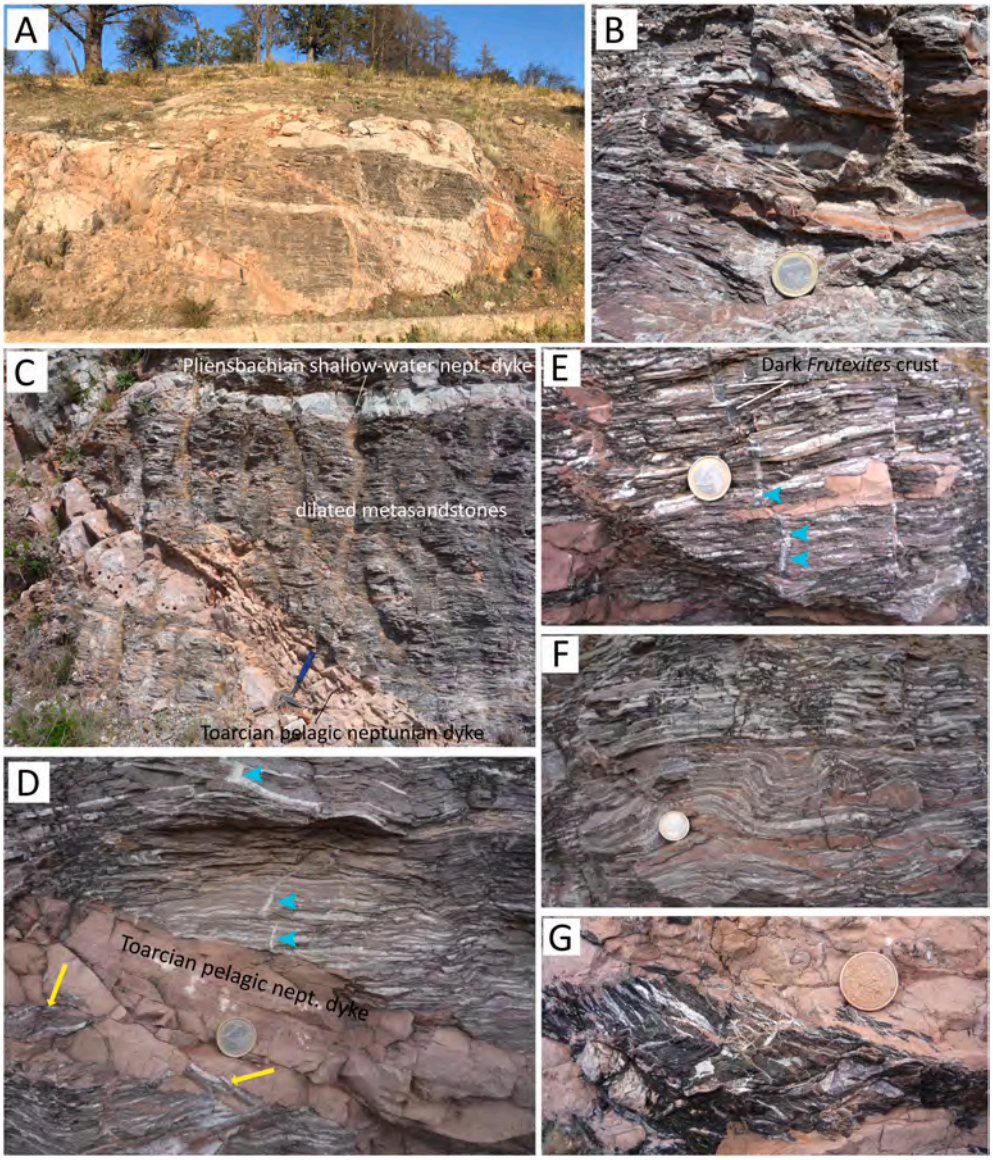

Fig. 2. –Field views of the main outcrop of metamorphic rocks dilated by pervasive calcite veins: A) Panoramic view of SP251 km9 outcrop; B) Outcrop view of the red veins consisting of micropeloidal facies filling the fractures; C) Detail of the metamorphic rocks cut by two generations of neptunian dykes with different compositions, *i.e.* Pliensbachian shallow-water carbonates and Toarcian pelagic mudstone/wackestone; D) Detail of calcite veins intersected by a Toarcian neptunian dyke. Blue arrows highlight calcite veins perpendicular to the cleavage, while yellow arrows denote fragments of the dyke wall torn and encased within pelagic sediment (crackle breccia). Significantly, the lithoclasts contain calcite veins; E) Detail of veins parallel to the cleavage planes intersected by a vertical vein, which also contains black *Frutexites* crusts; note Toarcian dyke running parallel to cleavage, cutting a vertical vein; F) Veins enhancing folds in the basement; G) Close-up of metasandstone lithoclast with veins (see Fig. 2B) embedded in the dyke.

Sometimes, these micritic laminae include trapped and bound grains mainly composed of coprolitic peloids and also, but less abundant, calcispheres (Fig. 3D and E). As seen in Fig. 3A, a symmetry plane is often observed within a sheet crack, with micrite encrusting the "roof" and "floor" and centripetal calcite crystal growth from both sides.

- Large radiaxial-fibrous calcite crystals (RFC) are characterized by the arrangement into isopachous bands (Fig. 4A and B) of individual crystals with lengths ranging from 300 to 400 μm up to 2400 μm and width of 100–300 μm (Fig. 4C and D). These crystals are characterized by a high angle between the c-axis and the dominant growth vector (length-slow character), and by undulate extinction.

The bands of RFC crystals bear few micrite intercalations at their base (Fig. 4A and B), passing to thinner RFC crystals densely alternating with micrite laminae (Fig. 4C and D). The growth direction of these crystals is symmetrical from both sides of the sheet-like cavities. The boundary between these two different generations can locally be marked by reddish, fringed, and irregular contact surfaces. The metasandstone at cavity boundaries also has a red/brown stain (Fig. 3B).

Besides the cleavage-parallel veins, also a network of 1–3 mm-thick calcite veins exists at a high angle with the former. These veins are dominantly characterized by the presence of RFC arranged, also in this case, into isopachous bands, 600–1400 μm thick.

4.3. Fe/mn mineralizations

Heavy minerals, dominantly Fe- and Mn-based and subordinately Zn-based, are very common and occur either in the host rock or in the calcite veins. They can occur as very thin films covering the calcite crystals (Fig. 5A) or as arborescent to dendritic patches (ca. 100–150 μm long) with irregular edges (Fig. 5B) encased within a sparry calcite

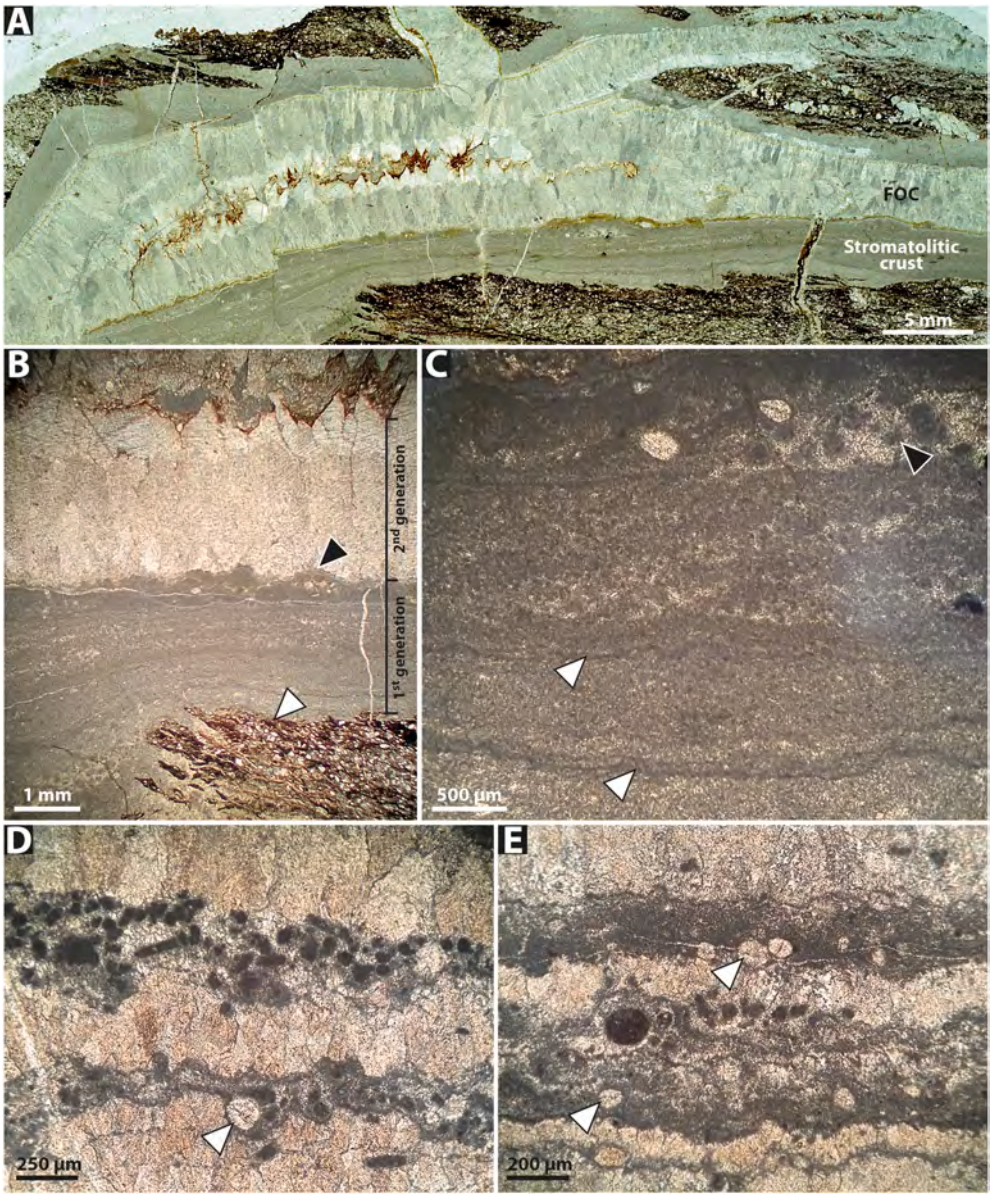

Fig. 3. A) Microphotograph showing the typical aspect of a cleavage-parallel calcite vein. The roof and floor show inward accretion of micritic stromatolite crusts, followed by the growth of radiaxial-fibrous calcite crystals (RFC) (left half of the picture); a subvertical vein traverses both the micrite and the upper calcitic crust (center); a lensoid cavity (left) shows oxidized crystal terminations and a micrite infilling; note red/brown-stained very fine metasandstone/siltstone at cavity walls; B) Enlargement of dilated cleavage plane showing a micritic stromatolite crust, overlain by RFC. Note the fringed and reddish fracture edges of the metamorphite host (white arrows) and micro-domes in the stromatolitic crusts (black arrow); C) Detail of the stromatolitic crusts showing the accretion of multiple generations of dark micritic laminae commonly having a dominant flat to undulated fabric (white arrows), alternating with peloidal laminae (black arrow); (D) and (E) Detail of two laminae composed of coprolitic peloids and calcispheres (white arrows).

cement. These latter are known as *Frutexites*-like structures (e.g. Maslov, 1960; Hofmann, 1969; Reitner, 1993).

Both the *Frutexites* structures and the thin films revealed a variable chemical composition ranging from Mn-dominant (e.g., MnO 95.5 wt % vs Fe_2O_3 2.5 wt %) to Fe-dominant (e.g., Fe_2O_3 87.1 wt % vs MnO 0.0 wt %) (Table 1). Despite morphological similarities, their varying composition is evident in the EDS, optical color and in their Raman spectra. The Mn-*Frutexites* and Mn-films show a dark to light-grayish color (Figs. 5 and 6) and are characterized by a main large and sharp Raman peak at 636 cm^{-1} ascribable to todorokite (an anhydrous manganese oxide) (Fig. 5). The Fe-*Frutexites* and Fe-films instead have a reddish to brownish color (Figs. 5 and 7) and a Raman spectrum with a main peak at 290 cm^{-1} and secondary peaks at 222, 408, 607 and 1320 cm^{-1} suggesting the presence of hematite (Fig. 5). For both mineral phases, additional smaller peaks occur in the higher wavenumber region, assignable to C-C, C-H and O-H stretching vibrations.

Both *Frutexites* and the films are well distinguishable from the surrounding minerals, generally calcite crystals (Fig. 8A and B). The Fe/Mn mineralizations are formed by the tight aggregation of small nanospheres (ca. 100–200 nm) grading to thin acicular crystals (ca. 2–3 µm long; Fig. 8C and D) associated with widespread organic matter, such as small filaments and thin sheet-like membranes (Fig. 8E and F). Moreover, the presence of microspheres (ca. 4 µm in diameter) bonded to form small chains (ca. 10–20 µm long) is very common. These microspheres are formed by the aggregation of nanocrystals and are commonly associated with organic matter remains (Fig. 8G and H).

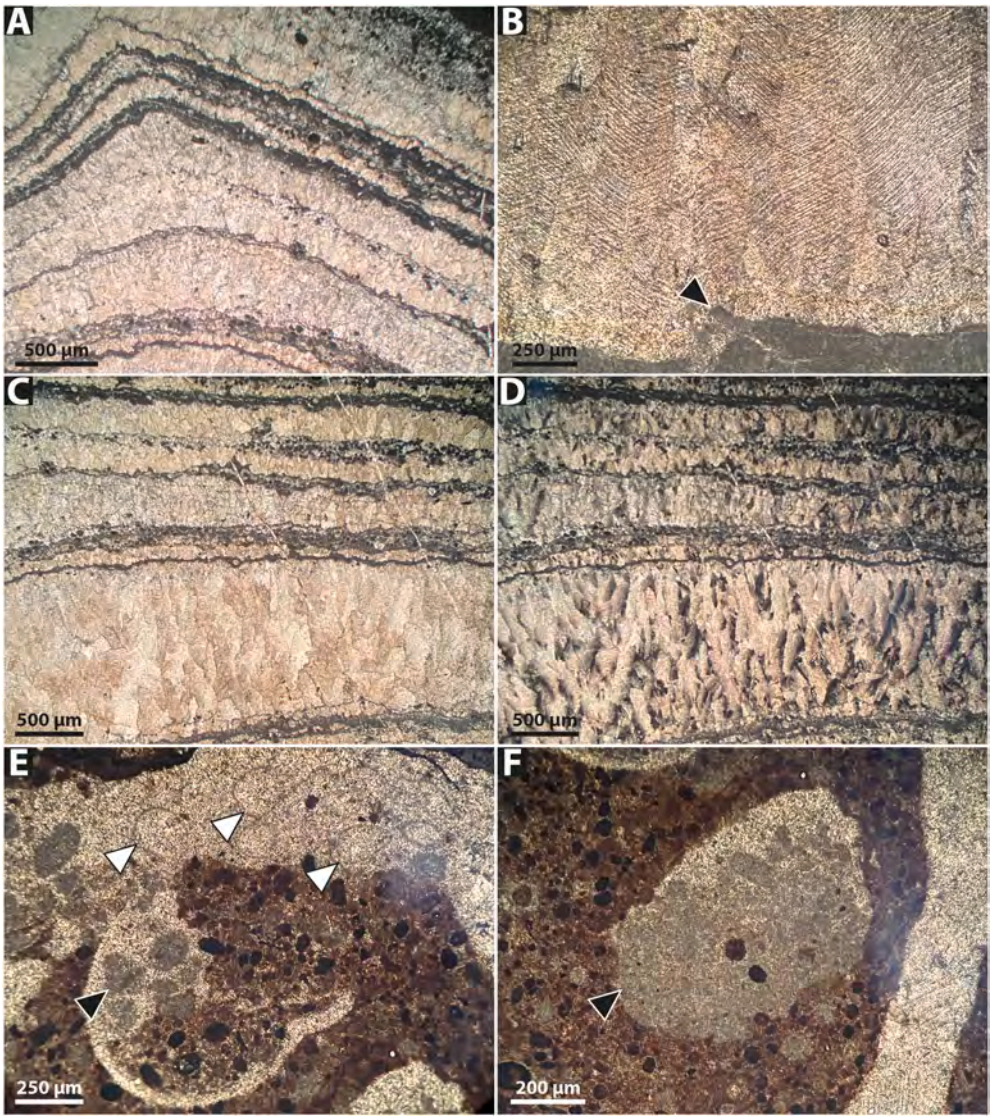

Fig. 4. A) Isopachous bands of radiaxial-fibrous calcite crystals (RFC) alternated to thin micrite laminae; B) Detail of the radiaxial-fibrous calcite crystals characterized by a high angle between the c-axis and the dominant growth vector and developing above a stromatolitic crust with an irregular top border (black arrow); (C) Plane and (D) cross-polarized view of the RFC with different thicknesses. Note the thicker RFC at the base and thinner RFC at the top, forming dense alternations with microbial laminae; E) accumulation of coprolitic peloids (black arrow) and calcispheres (white arrows) along a vein; F) Geopetal structure marked by micrite peloids accumulation (black arrow).

4.4. C, O, and clumped isotopes

The veins are characterized by $\delta^{13}C$ values between +2.7 and + 3.5 ‰, and $\delta\ ^{18}O$ values between −2.0 and −0.57 ‰ VPDB (Fig. 9), while calculated $\delta\ ^{18}O$ of the fluids are between +0.6 and + 3.6 ‰ VSMOW (Fig. 9). Such values are consistent with those of Pliensbachian seawater (Armendáriz et al., 2013; Fernandez et al., 2021), while the measured Δ_{47} temperature is bracketed between 33.6 and 43.8 °C (Fig. 10).

One of the limitations of carbonate clumped isotope thermometry is the potential alteration of the initial temperature due to solid-state bond reordering (e.g., Passey and Henkes, 2012; Henkes et al., 2014; Stolper and EIler, 2015; Hemingway and Henkes, 2021), potentially resulting in apparent T_{47} values higher than the original crystallization temperature. At Caloveto, burial modeling indicated peak temperatures not exceeding 125 °C over a maximum duration of 6 Myr (Innamorati, 2022), which should only cause minimal solid-state bond reordering equivalent at most to +0.5 °C (Hemingway and Henkes, 2021).

Alternatively, high apparent Δ_{47} temperatures could also be attributed to diagenetic dissolution and recrystallization during deep burial. However, the primary structures observed within calcite veins and the low temperatures measured in our samples lead us to exclude this possibility.

5. Discussion

5.1. Origin of calcite veins

Pervasive generation of calcite veins is generally regarded as a syntectonic process, wherein the veins form as a result of fluid circulation occurring from shallow (e.g. Al-Aasm et al., 1995) up to deep burial conditions, filling and eventually enlarging fractures through a crack-seal mechanism (e.g. Hilgers and Urai, 2005). However, in the studied samples a different process of formation, involving the carbonate crystallization mediated by microbial communities at the rock/sea-water interface, is inferred. To the best of our knowledge, we document for the first time a bio-diagenetic process fostering carbonate crystallization in low grade metamorphic host rocks in a rocky shore environment. Microbial colonization took place in cryptic environments

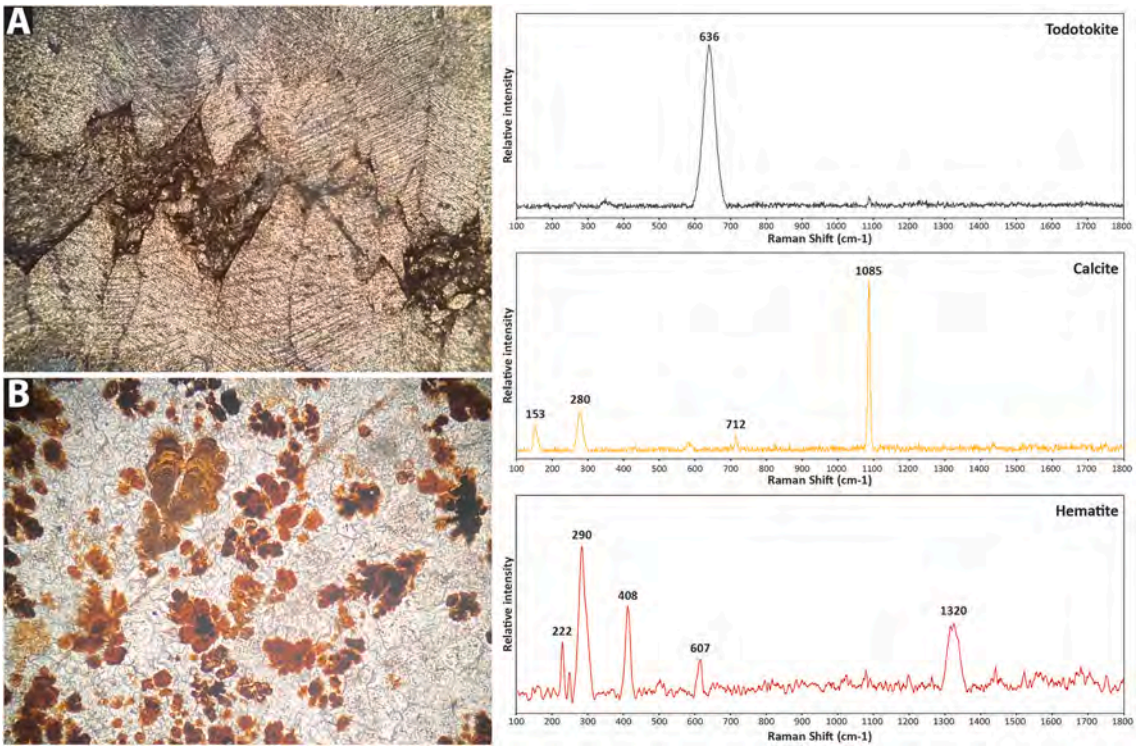

Fig. 5. A) Thin brownish Fe- and Mn-based film covering the radiaxial-fibrous calcite crystals, lining a cavity infilled with microclastic micrite; B) Arborescent to dendritic patches of *Frutexites*-like structures within a whitish sparry calcite cement. The Raman spectra of Mn-*Frutexites* (todorokite), Fe-*Frutexites* (hematite) and the sparry calcite cement surrounding them is reported on the right.

Table 1
SEM-EDS data of the main oxides found within the *Frutexites* and associated minerals.

Sample	MnO (%)	Fe_2O_3 (%)	CaO (%)	CuO (%)	CO_2 (%)	MgO (%)	K_2O (%)	ZnO (%)
Ca-1	43.9	0.9	3.8	0.3	51.0	0.1		
Ca-2	95.5	2.5	1.1	0.9				
Ca-3	94.6	1.4	3.6	0.4				
Ca-4	69.2	19.8	5.9			3.6	1.5	
Ca-5		73.5	23.5			3		
Ca-6		87.1	11.7				1.2	
Ca-7	31.8	21.5	5.4			8.3	9.7	23.3
Ca-8	21.2	22.9	8.8			10.2	11.9	25
Ca-9	24.5	21.4	8			11	14.6	20.5
Ca-10			6.3					93.7
Ca-11	5	59.7	9.3					26
Ca-12		79.3	5.8			4.6	10.3	

adjacent to emergent land as the Caloveto area, described in this paper, was a small island or promontory during the initial stages of flooding of a continental margin (Santantonio and Fabbi, 2020). We exclude that dilation of cleavage planes may have predated calcite precipitation and that calcite crystals filled pre-existing cavities as most of the sheet cracks do not contain coarse/very coarse sand- or granule-size carbonate allochems, as it would have been expected in a shallow water high-energy setting where well-washed carbonate sediment grew soon after the initial flooding (lower Caloveto fm.; Santantonio and Fabbi, 2020). This suggests that the cavities were originally unfit, due to their reduced width, to host any coarse sediment, and their enlargement must have occurred by calcite crystallization (see paragraph 4.3).

Away from the unconformable contact with the Mesozoic carbonates, the Paleozoic low-grade metamorphic rocks do not host calcite veins. This implies that the formation of calcite veins is not related to tectonic (e.g., exhumation) processes, which would otherwise affect the entire volume of rock and not just a very narrow band, and that the microbial colonization occurred in a precise environment, along a Jurassic coastline.

The relatively high sea-water temperatures derived from clumped isotopes (Fig. 10) are not surprising when considering a very shallow-water environment such as a rocky coastline setting with tide pools where warmer waters, compared to the open ocean, occur also as a consequence of the contact with dark rocks heated by the sun at tropical latitudes, in an environment which would also be conducive to evaporative enrichment of waters. Additionally, recent modeling of Pliensbachian-Toarcian oceanic temperatures (Fernandez et al., 2021; Letulle et al., 2022) reveals mean values higher than those previously reported (e.g., Shackleton and Kennett, 1975).

It is also worth noting that across the Longobucco Basin, the metamorphic rocks do not exhibit dilation (with calcite veins) at contacts with deep-water siliciclastic deposits (e.g., Pliensbachian-Toarcian marls and turbidites) taking place along deeper escarpment tracts of the rift-basin margin. Here, the basement locally displays neptunian dykes made of pelagic carbonate, testifying that in different conditions than those described above (*i.e.,* along escarpments lying in deeper water) open fissures were filled with marine sediment and not by a distinctive array of different types of calcite crystals microfabrics.

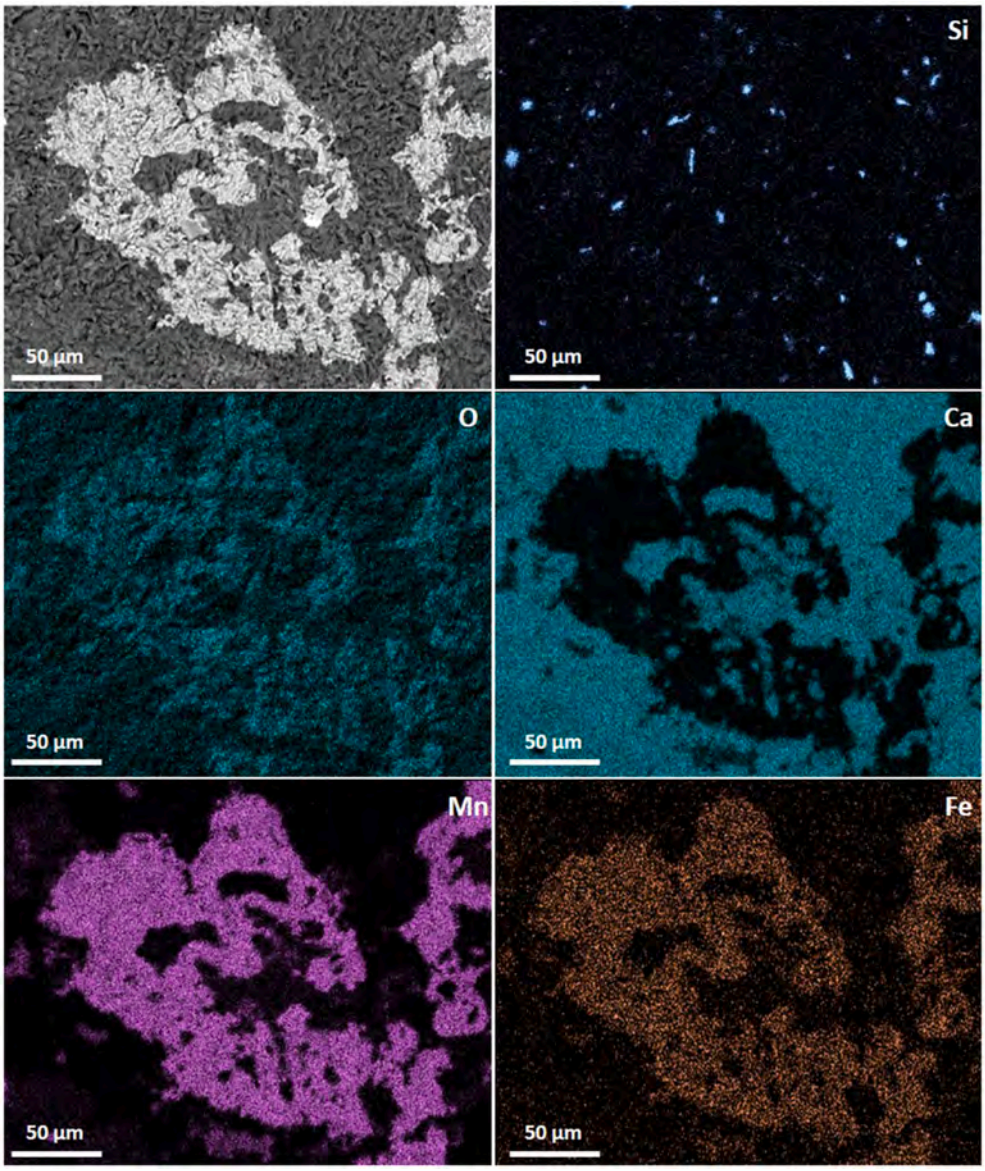

Fig. 6. Mn-*Frutexites* chemical map showing the main elemental distributions (Si, O, Ca, Mn, Fe). Note the higher Mn content than Fe in the *Frutexites*-like structure that is surrounded by calcite as revealed by the Ca content. Si is instead randomly dispersed.

As a consequence of the above evidence, we interpret the dilation of low-grade metamorphic rocks as the first known case of microbially-induced growth of calcite crystals at the rock/sea-water interface, able to displace cleavage planes of metamorphic host-rock through the force of crystallization.

5.2. *Microbial influence on the stages of vein formation*

The inferred sequence of events of calcite vein formation (Fig. 11) is complex and characterized by different genetic processes, almost all involving a microbial influence. The oldest evidence of mineralization of cleavage planes is traced back to the pre-Pliensbachian, when the basement rocks were exposed to subaerial conditions. As such, these rocks were subjected to the action of acidic meteoric fluids. This could have favored the dissolution of carbonate cements in the metasandstones and the chemical weathering of terrigenous grains, resulting in the precipitation of newly formed Fe-Mn minerals. These processes are witnessed by the ubiquitous presence of irregular, reddened, and etched cavity walls in the studied samples (Fig. 3A and B). In addition, weathering of the host rock could have directly influenced the chemistry of the cleavage-plane microenvironments, since it is an important source of dissolved nutrients, resulting in the alkalization of circulating water (Reitner, 1993; Balter et al., 2008; Percival et al., 2019). Under these conditions a microbial community could have thrived, inducing the precipitation of Fe-Mn oxyhydroxides such as the todorokite and hematite minerals forming the *Frutexites* structures (Fig. 5). These latter are dominant near the cavity walls, and gradually disappear away from them within the host rock (Fig. 3A).

The involvement of a microbial community in the mineralization processes described above is revealed by the very common presence of filamentous and sheet-like organic matter remains (Fig. 8E and F), and by associated *Frutexites* showing a crystalline hierarchical structure characterized by the tight aggregation of small nanospheres grading to thin acicular crystals (Fig. 8C and D), representing the typical aspect of a biotic mineral product (Niederberger and Colfen, 2006). According to this interpretation, the mineralization process could have been initiated on nucleation sites of the bacterial sheaths or extracellular polymeric substances (EPS) that adsorbed the available metal ions (Fe, Mn, and also Zn), oxidizing them upon decay of the organic substrate (Frankel and Bazylinski, 2003; Little et al., 1997). This induced the local

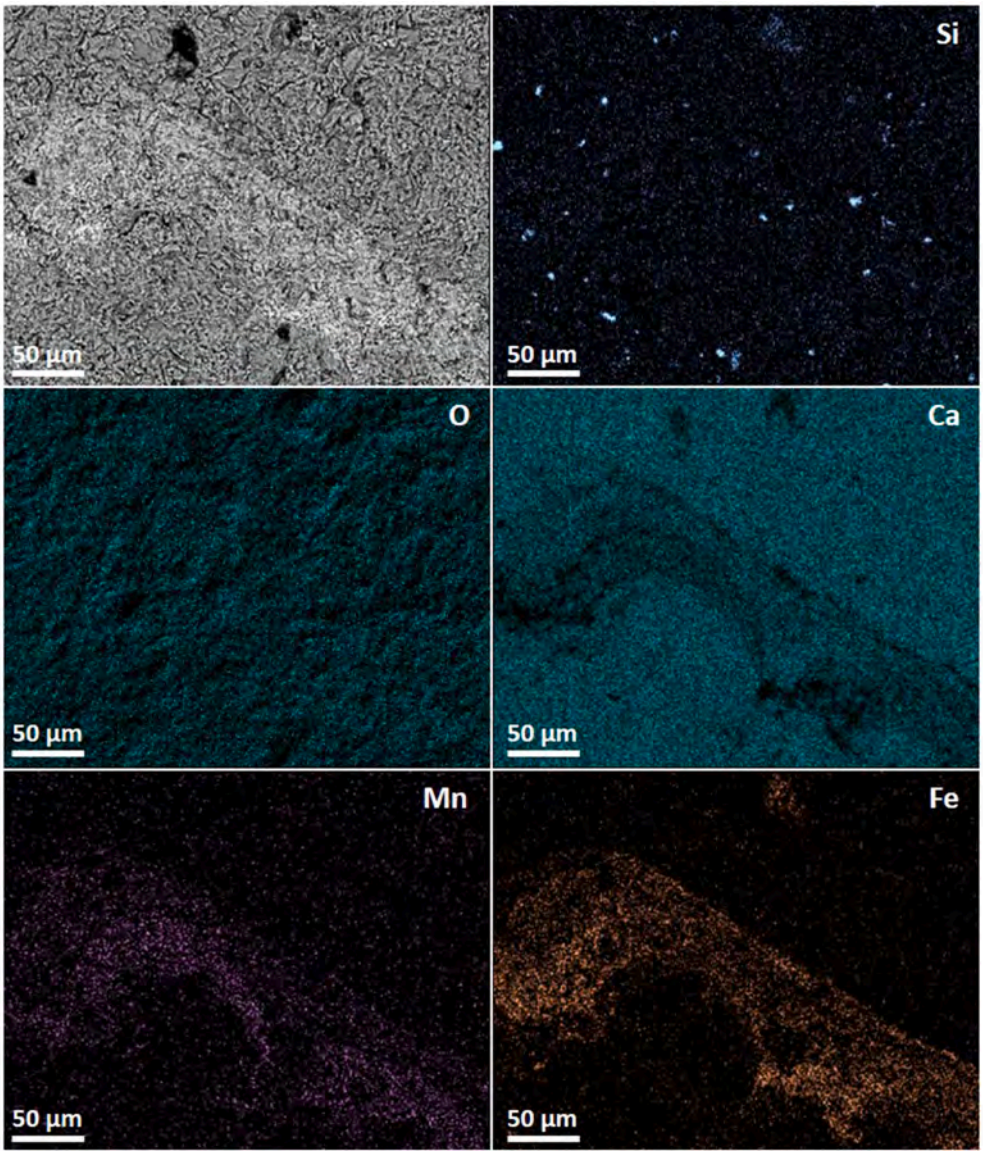

Fig. 7. Fe-lamina chemical map showing the main elemental distributions (Si, O, Ca, Mn, Fe). Note the higher Mn content than Fe in the lamina, surrounded by calcite as revealed by the Ca content. Si is again randomly dispersed.

precipitation of the Fe and Mn oxyhydroxides (Frankel and Bazylinski, 2003; Braissant et al., 2007; Champenois et al., 2023). The presence of Zn-based microspheres (ca. 4 µm in diameter), formed by the aggregation of nanocrystals and bonded to form small chains (ca. 10–20 µm long) resembling bacterial forms, also suggests the diversity of the microbial community colonizing the studied environment.

Subsequently, marine flooding was accompanied by rift-related extension at the Sinemurian/Pliensbachian boundary. A new microbial community colonized the "roof" and "floor" of the cleavage planes of the host rock, producing stromatolitic crusts (Fig. 3B and C) that represent the first vein-filling generation (Fig. 3B). These crusts commonly show the typical fabric of microbialites (Riding, 2000), which can develop over a wide range of settings, from hypersaline lakes (e.g., Perri et al., 2018; Gindre-Chanu et al., 2020; Borrelli et al., 2021) to shallow-to deep-water marine environments (e.g., Perri et al., 2019, 2024; Santagati et al., 2024). Within the stromatolitic laminae, the presence of detrital peloids (coprolites) and calcispheres (Fig. 3D and E) indicates a fully marine environment. Calcispheres are enigmatic microfossils that are very common in Paleozoic shallow-water marine deposits (Kazmierczak and Kremer, 2005), although they were also reported from Mesozoic deeper-water pelagic successions (Dal Corso et al., 2021). The stromatolites must have formed in a shallow-water environment linked with marine transgression, which would shortly after be conducive to the growth of reefs attached to the Paleozoic bedrock. Such environmental setting should have been characterized by high oxygenation, in sharp contrast to the sub-oxic to anoxic conditions governing the *Frutexites* formation in restricted microenvironments (e.g., Kazmierczak and Kempe, 2006; Cavalazzi et al., 2007).

The stromatolitic crusts locally display oxidized peripheries (Fig. 3B and C), which suggests the circulation of meteoric waters, possibly linked with an ephemeral relative sea-level drop.

The second generation of vein filling consists of radiaxial-fibrous calcite crystals (RFC) (Fig. 4A and B), that are generally considered direct marine precipitates from sea-water (Hood et al., 2011; Zhao et al., 2021; Hu et al., 2022), and interlayered micrite laminae with common calcispheres and peloids. The precipitation of RFC is generally fast and can be ruled over by a wide range of fluids; controlling factors include, among others, type of substratum, fluid temperature, and biogenic influence (e.g. Kendall, 1985; Russo et al., 2006a,b; Van der Kooij et al., 2007; Reinhold and Kaufmann, 2010). The micrite inter-laminae

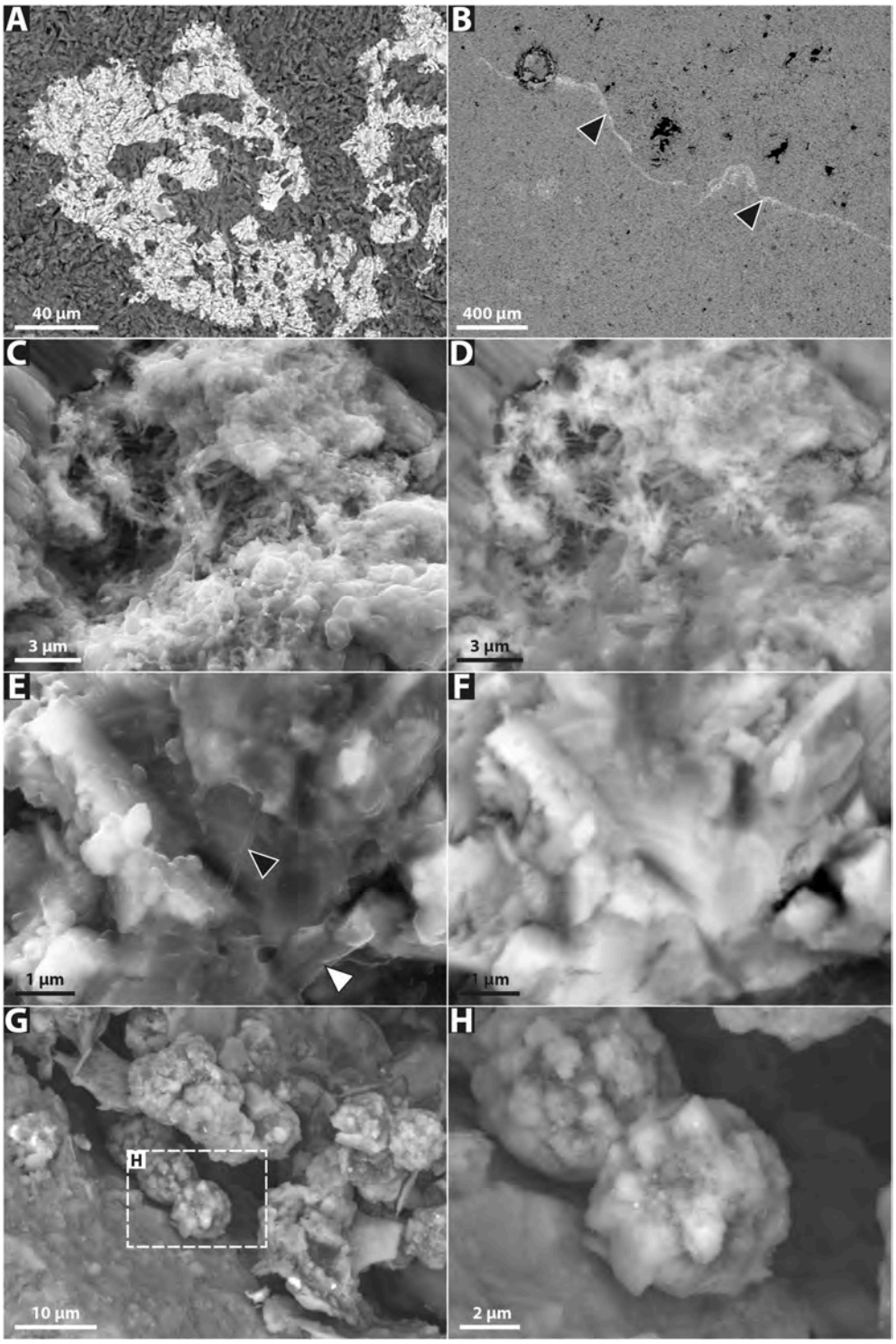

Fig. 8. SEM photomicrographs of the Fe-, Mn-*Frutexites*. A) Typical aspect of Mn-*Frutexites* showing an arborescent morphology with fringed and irregular borders. Note the lighter backscattered color of the *Frutexites* with respect to the surrounding calcite; B) Thin Fe-dominated film covering the irregular border of a calcite vein (black arrows); (C) Secondary electrons and (D) backscattered image of the Fe/Mn mineralizations characterized by the tight aggregation of small nanospheres grading to thin acicular crystals; (E) Secondary electrons and (F) backscattered image of sheet-like (white arrow) and filamentous (black arrow) organic matter; G) Zn-based minerals forming microspheres bonded to form small chains is very common; H) Detail of a Zn-microsphere formed by the aggregation of nanocrystals.

document the development of biofilms, binding minute debris such as peloids and calcispheres. A greater density of micritic interlaminae is generally correlated with a reduced thickness of the RFC bands (Fig. 4C and D). These alternations could mark shifts in the microenvironmental conditions, reflecting changes in fluid availability and/or composition.

Ghosts of peloids are often found within the RFC crystals (Fig. 3E), indicating that the growth of calcite bands could be the result of recrystallization of the micritic biofilms.

5.3. Vein enlargement process

There is ample evidence that the confined growth of minerals creates

Sample averages

Sample	N	Yield (%)	$\delta^{13}C_{VPDB}$	$\delta^{18}O_{VSMOW}$ (CO_2)	$\delta^{18}O_{VPDB}$ (calcite*)	Δ_{47} (I-CDES)	± SE	(± 95 %)	SD	p-value (Levene)
ETH-1	6	100	2.05	37.05	−2.16	0.2052			0.0083	
ETH-2	8	99	−10.17	19.87	−18.69	0.2085			0.0064	
ETH-3	13	95	1.70	37.44	−1.79	0.6132			0.0074	
ETH-4	3	101	−10.25	19.71	−18.85	0.4511			0.0113	
C1H	3	88	3.53	38.18	−1.08	0.5564	± 0.0054	(± 0.0110)	0.0096	0.82
C2H	3	89	2.85	37.56	−1.67	0.5685	± 0.0054	(± 0.0110)	0.0106	0.67
C3H	3	93	3.16	37.90	−1.35	0.5435	± 0.0054	(± 0.0110)	0.0050	0.49
C3V	3	95	3.20	38.71	−0.57	0.5417	± 0.0054	(± 0.0110)	0.0071	0.80
C4H	3	93	2.71	37.22	−2.00	0.5544	± 0.0054	(± 0.0110)	0.0025	0.21
PCH1	3	86	3.35	38.08	−1.17	0.5620	± 0.0054	(± 0.0110)	0.0058	0.59

Fig. 9. – Results of C, O and clumped isotopes analysis. Where not specified, values are expressed in ‰.

Temperature and water $\delta^{18}O$ reconstructions

Sample	N	Δ_{47} (‰ ± 95 %)	T_{47} (°C ± 95 %)	Water $\delta^{18}O_{VSMOW}$ (‰ ± 95 %) *Kim & O'Neil* [1997]	Water $\delta^{18}O_{VSMOW}$ (‰ ± 95 %) *Daëron et al.* [2019]
C1H	3	0.5564 ± 0.0110	38.1 ± 4.2	+3.9 ± 0.8	+2.1 ± 0.8
C2H	3	0.5685 ± 0.0110	33.6 ± 4.0	+2.4 ± 0.8	+0.6 ± 0.7
C3H	3	0.5435 ± 0.0110	43.1 ± 4.4	+4.5 ± 0.8	+2.7 ± 0.8
C3V	3	0.5417 ± 0.0110	43.8 ± 4.4	+5.4 ± 0.8	+3.6 ± 0.8
C4H	3	0.5544 ± 0.0110	38.9 ± 4.2	+3.1 ± 0.8	+1.3 ± 0.8
PCH1	3	0.5620 ± 0.0110	36.0 ± 4.1	+3.4 ± 0.8	+1.6 ± 0.8

Fig. 10. – Temperature and water $\delta^{18}O$ reconstructions.

forces that can damage solid materials (Taber, 1916; Flatt et al., 2007; Noiriel et al., 2010; Li et al., 2017). Laboratory experiments reproduced the inorganic growth of crystals (NaCl, KCl, $CaCO_3$), revealing how the force of crystallization can cause breakup and subsequent fracture sealing in rocks (Espinosa-Marzal and Scherer, 2010; Noiriel et al., 2010). In natural environments, hydrothermal aragonite veins up to 27 cm thick are known to have caused the uplift of a travertine mound, only due to the force of crystallization (Gratier et al., 2012).

An equilibrium boundary exists between destructive and non-destructive crystal growth, depending on the confinement/force of crystallization ratio (Li et al., 2017). This is particularly effective for porous rocks or loose sediments, where fluids circulate easily (Noiriel et al., 2010). In metasandstones with low permeability, the preferential paths for fluid circulation would be pre-existing fractures and/or cleavage planes, which is our case.

The enlargement of pre-existing cleavage-related discontinuities, including the folded portions deformed during the Hercynian orogeny (Fig. 2F), also caused the cracking of the host rock along new fractures at a high angle with the cleavage. In thin sections, these fractures are seen to originate from the sheet-like fissures. They truncate both the stromatolitic crusts and the cleavage-parallel calcite, then host themselves the growth of RFC crystals (Fig. 3A). The truncation of earlier crusts, through the progression of the same continuous process that produced them, is an indication that the mineralization of microbial communities was a quite fast process.

The dilation produced by the force of crystallization exerted against the walls of cleavage planes could locally result in the opening of sheet-like/lensoid cavities lateral to the zone of contact of RFC bands having opposite growth directions (Fig. 3A). Very thin Fe-Mn crusts lining crystal terminations might either indicate the local circulation of meteoric waters during a sea-level drop or represent mineralized biofilms in marine conditions.

5.4. *Markers of ancient basin margins*

In the Jurassic rift basins of the Western Tethys, basin margins often corresponded to submarine escarpments rooted in extensional faults, defining a complex architecture of structural highs and lows in a pelagic environment. As the primary architectures were disrupted during later phases of plate convergence and/or crustal stretching, identifying exhumed palaeoescarpment tracts in the field, and restoring the original geometries of the rift, require undoing the younger tectonic overprints, paired with dedicated methods of mapping and facies analysis (Santantonio, 1993).

While a set of field-based criteria for the analysis of submarine palaeoescarpments has been established for the carbonate-dominated southern margins of the Western Tethys (e.g. Northern Apennines: Galluzzo and Santantonio, 2002; Carminati and Santantonio, 2005; Santantonio et al., 2017, 2024; Cipriani et al., 2019), inverted rift basins where the deeper-water sedimentary successions of hangingwall basins abut the crystalline or metamorphic basement pose different problems, as for example the nature and geometry of contacts can be equivocal in the absence of bedding in the substrate. This is the case with the European-Iberian margin of the Western Tethys (Calabria: Santantonio et al., 2016; Santantonio and Fabbi, 2020), where the basin-margin onlap contacts of sedimentary rocks with the basement had in some instances been previously mapped as thrust fault contacts, and were later reinterpreted by Innamorati and Santantonio (2018).

In the case example described in this paper, the basin-margin zones where veining and dilation of the low-grade metamorphic rocks took place are interpreted to correspond to the most surficial portions of escarpments, lying in shallow water in the Pliensbachian, which continued downwards into the deep water as unroofing of the basement along normal faults progressed (Fig. 11). As such, their recognition defines the local architecture of the rift, representing an additional tool in basin analysis.

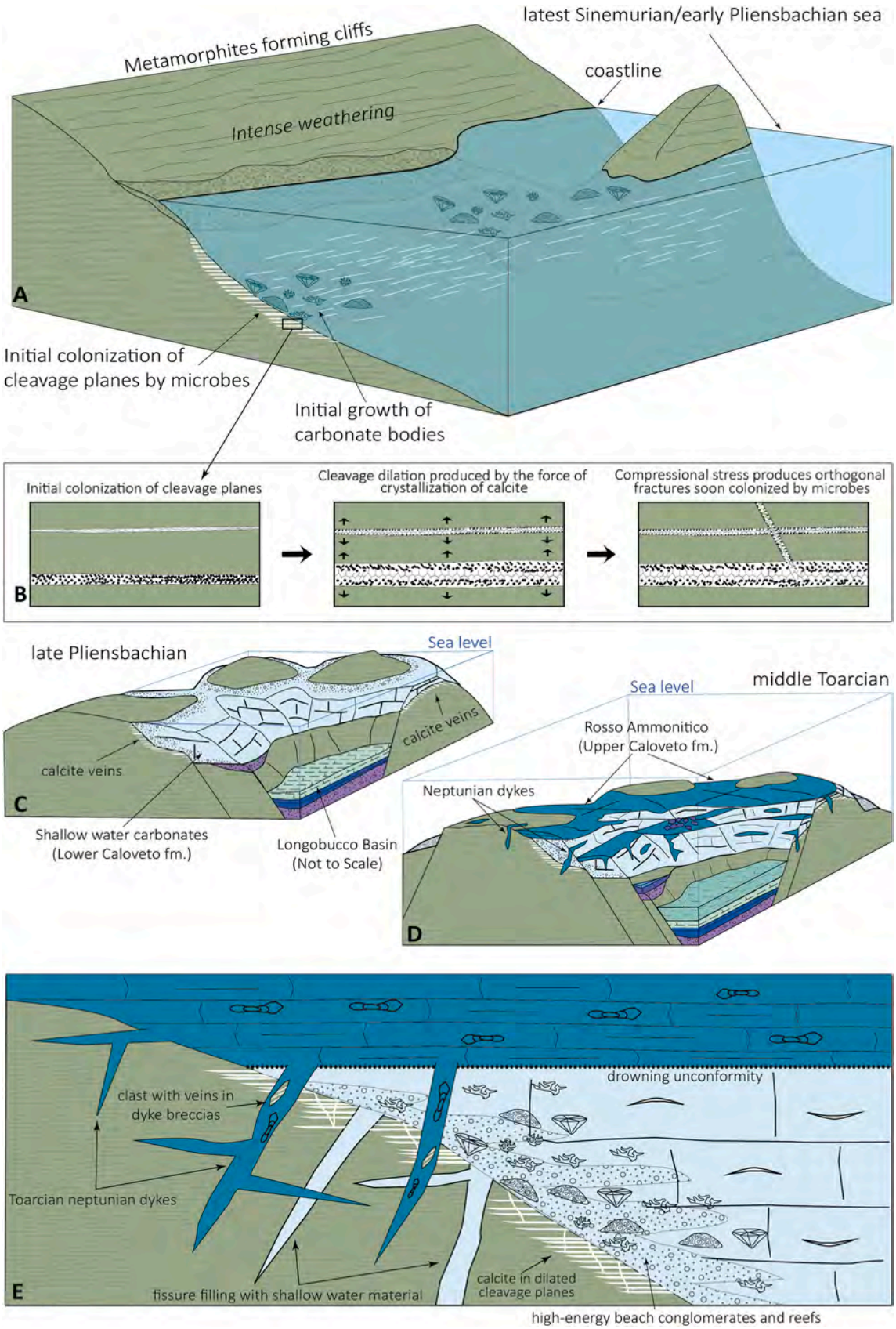

Fig. 11. – Latest Sinemurian/middle Toarcian evolution of the Longobucco Basin margin at Caloveto. A. conditions at the Sinemurian/Pliensbachian boundary; B. phases of cleavage colonization and vein opening; C, D. evolution of the Caloveto highs in the Pliensbachian and Toarcian (Modified from Santantonio and Fabbi, 2020); E. Ideal section representing the relationships between the veined metamorphic basement and sedimentary cover in the middle Toarcian.

6. Conclusions

Although calcite veins in deeply buried metamorphic and crystalline rocks are known to be the product of microbial activity, the occurrences discussed in this article document microbially-induced calcite growth at the rock/sea-water interface, leading to volume increase and cracking of the exposed host rock. O and C isotopic values are consistent with precipitation from evaporatively fractionated seawater, at temperatures of ~44 °C at most. The swollen phyllites occur exclusively at stratigraphic contacts (steeply dipping unconformities) between the shallow-water, locally reefal, carbonates, and the basement. As such, they define the margins of the Longobucco rift basin, and of the structural highs which existed within it. Individual palaeomargin tracts with microbially-modified metamorphites can be mapped continuously for several kilometers. Wherever the Jurassic rift faults cut across the middle/upper crust boundary in the rotated Palaeozoic basement, evidence for the lateral continuation of the palaeomargin is solely provided by the onlap contacts of the basin-fill formations, due to the inability of granitoid rocks to host the same processes.

Based on this work, the seemingly odd occurrence of metasandstones with calcite bands could be taken as an evidence, in geologic regions with a comparable palaeogeographic/palaeotectonic setting, of the exposure of metamorphic rocks in a shallow-water carbonate environment. In poly-deformed regions like Calabria, the presence of a band of veined metasandstones alone, even in the absence of a preserved contact with the carbonates due to damaging by younger faults and/or modern erosion, represents a previously unexploited marker of exhumed basin-margin tracts.

CRediT authorship contribution statement

S. Fabbi: Writing – review & editing, Writing – original draft, Visualization, Validation, Investigation, Data curation, Conceptualization. **M. Borrelli:** Writing – review & editing, Writing – original draft, Visualization, Investigation, Formal analysis, Data curation. **G. Innamorati:** Writing – review & editing, Writing – original draft, Investigation, Data curation, Conceptualization. **L. Aldega:** Writing – review & editing, Validation, Methodology, Funding acquisition, Formal analysis, Data curation. **M. Daëron:** Writing – review & editing, Validation, Methodology, Formal analysis. **E. Perri:** Writing – review & editing, Writing – original draft, Visualization, Validation, Methodology, Investigation, Data curation. **M. Santantonio:** Writing – review & editing, Writing – original draft, Validation, Supervision, Methodology, Investigation, Funding acquisition, Data curation, Conceptualization.

Declaration of competing interest

The authors declare that they have no known competing financial interests or personal relationships that could have appeared to influence the work reported in this paper.

Data availability

Data will be made available on request.

Acknowledgments

This work has been supported by “Progetti di Ateneo” 2020 to Luca Aldega, and Progetti di Ateneo 2018; 2019 to Massimo Santantonio.

References

Al-Aasm, I.S., Coniglio, M., Descrochers, A., 1995. Formation of complex fibrous calcite veins in upper triassic strata of wrangellia terrain, British columbia, Canada. Sediment. Geol. 100, 83–95.

Armendáriz, M., Rosales, I., Bádenas, B., Pinuela, L., Aurell, M., García-Ramos, J.C., 2013. An approach to estimate Lower Jurassic seawater oxygen-isotope composition using δ18O and Mg/Ca ratios of belemnite calcites (Early Pliensbachian, northern Spain). Terra. Nova 25 (6), 439–445.

Balter, V., Renaud, S., Girard, C., Joachimski, M.M., 2008. Record of climate-driven morphological changes in 376 Ma Devonian fossils. Geology 36 (11), 907–910.

Bernasconi, M.P., Cefalà, M., Perri, E., 2015. Mid-latitude coralgal bioconstruction and endolithic microbialites: environmental significance during Quaternary climate variations. Facies 61, 1–18.

Bernasconi, S.M., Daëron, M., Bergmann, K.D., Bonifacie, M., Meckler, A.N., Affek, H.P., Anderson, N., Bajnai, D., Barkan, E., Beverly, E., Blamart, D., Burgener, L., Calmels, D., Chaduteau, C., Clog, M., Davidheiser-Kroll, B., Davies, A., Dux, F., Eiler, J., Elliot, B., Fetrow, A.C., Fiebig, J., Goldberg, S., Hermoso, M., Huntington, K. W., Hyland, E., Ingalls, M., Jaggi, M., John, C.M., Jost, A.B., Katz, S., Kelson, J., Kluge, T., Kocken, I.J., Laskar, A., Leutert, T.J., Liang, D., Lucarelli, J., Mackey, T.J., Mangenot, X., Meinicke, N., Modestou, S.E., Müller, I.A., Murray, S., Neary, A., Packard, N., Passey, B.H., Pelletier, E., Petersen, S., Piasecki, A., Schauer, A., Snell, K.E., Swart, P.K., Tripati, A., Upadhyay, D., Vennemann, T., Winkelstern, I., Yarian, D., Yoshida, N., Zhang, N., Ziegler, M., 2021. InterCarb: a community effort to improve inter-laboratory standardization of the carbonate clumped isotope thermometer using carbonate standards. G-cubed 22 (5), e2020GC009592. https://doi.org/10.1029/2020GC009588.

Bernasconi, S.M., Müller, I.A., Bergmann, K.D., Breitenbach, S.F.M., Fernandez, A., Hodell, D.A., Meckler, A.N., Millan, I., Ziegler, M., 2018. Reducing uncertainties in carbonate clumped isotope analysis through consistent carbonate-based standardization. G-cubed 19, 2895–2914. https://doi.org/10.1029/2017GC007385.

Bontognali, T.R.R., Vasconcelos, C., Warthmann, R.J., Dupraz, C., Bernasconi, S.M., McKenzie, J.A., 2008. Microbes produce nanobacteria-like structures, avoiding cell entombment. Geology 36, 663–666.

Borrelli, M., Campilongo, G., Critelli, S., Ida, D.P., Perri, E., 2019. 3D nanopores modeling using TEM-tomography (dolostones-Upper Triassic). Mar. Petrol. Geol. 99, 443–452.

Borrelli, M., Perri, E., Critelli, S., Gindre-Chanu, L., 2021. The onset of the Messinian Salinity Crisis in the central Mediterranean recorded by pre-salt carbonate/evaporite deposition. Sedimentology 68, 1159–1197.

Borrelli, M., Santagati, P., Guerrieri, S., Perri, E., 2024. Mid-latitude microbial-mediated modern beachrock formation (Santa Maria di Ricadi - Southern Italy), vol. 63. Rendiconti Società Geologica Italiana. https://doi.org/10.3301/ROL.2024.25.

Bouillin, J.P., Bellomo, D., 1990. Les filons sédimentaires jurassiques de Longobucco-Caloveto (Calabre, Italie); application à l’étude des paléostructures d’une marge téthysienne. Geodin. Acta 4, 111–120.

Braissant, O., Decho, A.W., Dupraz, C., Glunk, C., Przekop, K.M., Visscher, P.T., 2007. Exopolymeric substances of sulfate-reducing bacteria: interactions with calcium at alkaline pH and implication for formation of carbonate minerals. Geobiology 5 (4), 401–411.

Brand, W.A., Assonov, S.S., Coplen, T.B., 2010. Correction for the 17O interference in δ(13C) measurements when analyzing CO2 with stable isotope mass spectrometry (IUPAC Technical Report). Pure Appl. Chem. 82 (8), 1719–1733. https://doi.org/10.1351/PAC-REP-09-01-05.

Burne, R.V., Moore, L.S., 1987. Microbialites; organosedimentary deposits of benthic microbial communities. Palaios 2, 241–254.

Carminati, E., Santantonio, M., 2005. Control of differential compaction on the geometry of sediments onlapping paleoescarpments: insights from field geology (Central Apennines, Italy) and numerical modeling. Geology 33 (5), 353–356.

Cavalazzi, B., Barbieri, R., Ori, G.G., 2007. Chemosynthetic microbialites in the devonian carbonate mounds of hamar laghdad (Anti-Atlas, Morocco). Sediment. Geol. 200, 73–88.

Champenois, F., George, A.D., McNamara, K.J., Shaw, J., Cherdantseva, M., 2023. Contrasting morphology and growth habits of Frutexites in Late Devonian reef complexes of the Canning Basin, northwestern Australia. Geobiology 22 (1), e12579.

Cipriani, A., Fabbi, S., Lathuilière, B., Santantonio, M., 2019. A reef coral in the condensed Maiolica facies on the Mt Nerone pelagic carbonate platform (Marche Apennines): the enigma of ancient pelagic deposits. Sediment. Geol. 385, 45–60.

Daëron, M., Vermeesch, P., 2024. Omnivariant generalized least squares regression: theory, geochronological applications, and making the case for reconciled Δ47 calibrations. Chem. Geol. 647, 121881.

Daëron, M., 2021. Full propagation of analytical uncertainties in Δ47 measurements. G-cubed 22 (5). https://doi.org/10.1029/2020gc009592.

Daëron, M., Blamart, D., Peral, M., Affek, H.P., 2016. Absolute isotopic abundance ratios and the accuracy of Δ47 measurements. Chem. Geol. 442, 83–96. https://doi.org/10.1016/j.chemgeo.2016.08.014.

Dal Corso, J., Preto, N., Agnini, C., Hohn, S., Merico, A., Willems, H., Gianolla, P., 2021. Rise of calcispheres during the carnian pluvial Episode (late triassic). Global Planet. Change 200, 103453.

Dupraz, C., Strasser, A., 1999. Microbialites and micro-encrusters in shallow coral bioherms (middle to late oxfordian, Swiss jura mountains). Facies 40, 101–129.

Espinosa-Marzal, R.M., Scherer, G.W., 2010. Advances in understanding damage by salt crystallization. Accounts of Chemical Research 43, 897–905.

Fernandez, A., Korte, C., Ullmann, C.V., Looser, N., Wohlwend, S., Bernasconi, S.M., 2021. Reconstructing the magnitude of Early Toarcian (Jurassic) warming using the reordered clumped isotope compositions of belemnites. Geochem. Cosmochim. Acta 293, 308–327.

Flatt, R.J., Steiger, M., Scherer, G.W., 2007. A commented translation of the paper by CW Correns and W. Steinborn on crystallization pressure. Environmental Geology 52, 187–203.

Frankel, R.B., Bazylinski, D.A., 2003. Biologically induced mineralization by bacteria. Rev. Mineral. Geochem. 54 (1), 95–114.

Galluzzo, F., Santantonio, M., 2002. The sabina plateau: a new element in the mesozoic palaeogeography of central Apennines. Boll. Soc. Geol. Ital. 1, 561–588.
Gindre-Chanu, L., Borrelli, M., Caruso, A., Critelli, S., Perri, E., 2020. Carbonate/evaporitic sedimentation during the Messinian salinity crisis in active accretionary wedge basins of the northern Calabria, southern Italy. Mar. Petrol. Geol. 112, 104066.
Gratier, J.P., Frery, E., Deschamps, P., Røyne, A., Renard, F., Dysthe, D., Ellouz-Zimmerman, D., Hamelin, B., 2012. How travertine veins grow from top to bottom and lift the rocks above them: the effect of crystallization force. Geology 40, 1015–1018.
Heim, C., Quéric, N.V., Ionescu, D., Schäfer, N., Reitner, J., 2017. Frutexites-like structures formed by iron oxidizing biofilms in the continental subsurface (Äspö Hard Rock Laboratory, Sweden). PLoS One 12 (5), e0177542.
Hemingway, J.D., Henkes, G.A., 2021. A disordered kinetic model for clumped isotope bond reordering in carbonates. Earth Planet Sci. Lett. 566, 116962.
Henkes, G.A., Passey, B.H., Grossman, E.L., Shenton, B.J., Pérez-Huerta, A., Yancey, T.E., 2014. Temperature limits for preservation of primary calcite clumped isotope paleotemperatures. Geochem. Cosmochim. Acta 139, 362–382.
Hilgers, C., Urai, J.L., 2005. On the arrangement of solid inclusions in fibrous veins and the role of the crack-seal mechanism. J. Struct. Geol. 27, 481–494.
Hofmann, H.J., 1969. Stromatolites from the proterozoic animikie and sibley groups, ontario. Geol. Surv. Canada Pap (68–69), 1–77.
Hood, A.V., Wallace, M.W., Drysdale, R.N., 2011. Neoproterozoic aragonite-dolomite seas? Widespread marine dolomite precipitation in Cryogenian reef complexes. Geology 39, 871–874.
Hu, Y., Cai, C., Li, Y., Zhou, R., Lu, F., Hu, J., Ren, C., Jia, L., Zhou, Y., Lippert, K., Immenhauser, A., 2022. Upper Ediacaran fibrous dolomite versus Ordovician fibrous calcite cement: origin and significance as a paleoenvironmental archive. Chem. Geol. 609.
Innamorati, G., 2022. Tectonic-stratigraphic Evolution of the Longobucco Basin (NE Calabria), from Jurassic Extension to Cenozoic Compression: the Paludi Fm. Sapienza University of Rome. Ph. D. Thesis.
Innamorati, G., Santantonio, M., 2018. Evidence for extended hercynian basement and a preserved jurassic basin-margin tract in northern Calabria (southern Italy): the Longobucco Basin. Sediment. Geol. 376, 147–163.
Innamorati, G., Fabbi, S., Pignatti, J., Aldega, L., Santantonio, M., 2024. Early eocene tectono-sedimentary evolution of northern Calabria: hints from the paludi formation (Sila Greca). Italian Journal of Geosciences 143, 130–154. https://doi.org/10.3301/IJG.2024.07.
Kazmierczak, J., Kempe, S., 2006. Genuine modern analogues of Precambrian stromatolites from caldera lakes of Niuafʻoou Island. Tonga. Naturwissenschaften 93, 119–126.
Kaźmierczak, J., Kremer, B., 2005. Early post-mortem calcified Devonian acritarchs as a source of calcispheric structures. Facies 51, 554–565.
Kendall, A.C., 1985. Radiaxial fibrous calcite: a reappraisal. In: Schneidermann, N., Harris, P.M. (Eds.), Carbonate Cements, 36. SEPM Special Publication, pp. 59–77.
Kim, S.-T., Mucci, A., Taylor, B.E., 2007. Phosphoric acid fractionation factors for calcite and aragonite between 25 and 75 ◦C: revisited. Chem. Geol. 246 (3–4), 135–146. https://doi.org/10.1016/j.chemgeo.2007.08.005.
Konhauser, K., Riding, R., 2012. Bacterial Biomineralization. Fundamentals of Geobiology, pp. 105–130.
Lacelle, D., 2007. Environmental setting,(micro) morphologies and stable C–O isotope composition of cold climate carbonate precipitates-a review and evaluation of their potential as paleoclimatic proxies. Quat. Sci. Rev. 26 (11–12), 1670–1689.
Langone, A., Godard, G., Prosser, G., Caggianelli, A., Rottura, A., Tiepolo, M., 2010. P–T–t path of the Hercynian low-pressure rocks from the Mandatoriccio complex (Sila Massif, Calabria, Italy): new insights for crustal evolution. J. Metamorph. Geol. 28, 137–162.
Last, F.M., Last, W.M., Halden, N.M., 2010. Carbonate microbialites and hardgrounds from Manito Lake, an alkaline, hypersaline lake in the northern Great Plains of Canada. Sediment. Geol. 225 (1–2), 34–49.
Letulle, T., Suan, G., Daëron, M., Rogov, M., Lécuyer, C., Vinçon-Laugier, A., Reynard, B., Montagnac, G., Lutikov, O., Schlögl, J., 2022. Clumped isotope evidence for Early Jurassic extreme polar warmth and high climate sensitivity. Clim. Past 18 (3), 435–448.
Li, L., Kohler, F., Røyne, A., Dysthe, D.K., 2017. Growth of calcite in confinement. Crystals 7, 361.
Little, B.J., Wagner, P.A., Lewandowski, Z., 1997. Spatial relationships between bacteria and mineral surfaces. Rev. Mineral. 35, 123–160.
Maslov, V.P., 1960. Stromatolites. Trudy Geol. Inst. Akad. Nauk S.S.S.R. 41, 1–188.
Melim, L.A., Northup, D.E., Boston, P.J., Spilde, M.N., 2016. Preservation of fossil microbes and biofilm in cave pool carbonates and comparison to other microbial carbonate environments. Palaios 31 (4), 177–189.
Monty, C.L.V., 1982. Cavity or fissure dwelling stromatolites (endostromatolites) from Belgian Devonian mud mounds. Ann. Soc. Geol. Belg. 105, 343–344.
Myrow, P.M., Coniglio, M., 1991. Origin and diagenesis of cryptobiontic Frutexites in the chapel island formation (vendian to early cambrian) of southeast newfoundland, Canada. Palaios 6, 572–585.
Neubeck, A., Ivarsson, M., Broman, C., Lima-Zaloumis, J., Bach, W., Whitehouse, M., 2021. Carbon isotopic composition of Frutexites in subseafloor ultramafic rocks. Biogeochemistry 154 (3), 525–536.
Niederberger, M., Colfen, H., 2006. Oriented attachment and mesocrystals: non-classical crystallization mechanisms based on nanoparticle assembly. Phys. Chem. Chem. Phys. 8, 3271–3287.
Noiriel, C., Renard, F., Doan, M.L., Gratier, J.P., 2010. Intense fracturing and fracture sealing induced by mineral growth in porous rocks. Chem. Geol. 269, 197–209.
Passey, B.H., Henkes, G.A., 2012. Carbonate clumped isotope bond reordering and geospeedometry. Earth Planet Sci. Lett. 351, 223–236.
Percival, L.M.E., Selby, D., Bond, D.P.G., Rakocinski, M., Racki, G., Marynowski, L., Adatte, T., Spangenberg, J.E., Foellmi, K.B., 2019. Pulses of enhanced continental weathering associated with multiple Late Devonian climate perturbations: evidence from osmium-isotope compositions. Palaeogeogr. Palaeoclimatol. Palaeoecol. 524, 240–249.
Perri, E., Borrelli, M., Bernasconi, M.P., Gindre-Chanu, L., Spadafora, A., Critelli, S., 2019. Microbial-dominated carbonate depositional systems: a biosedimentary and stratigraphic reconstruction in the Late Triassic of Western Tethys (northern Calabria, Italy). Facies 65 (3), 31.
Perri, E., Borrelli, M., Heimhofer, U., Umbro, B., Santagati, P., Le Pera, E., 2024. Microbial dominated Ca-carbonates in a giant pliocene cold-seep system (crotone basin – south Italy). Sedimentology. https://doi.org/10.1111/sed.13192.
Perri, E., Borrelli, M., Spadafora, A., Critelli, S., 2017. The role of microbialitic facies in the micro-and nano-pore system of dolomitized carbonate platforms (Upper Triassic–Southern Italy). Mar. Petrol. Geol. 88, 1–17.
Perri, E., Słowakiewicz, M., Perrotta, I.D., Tucker, M.E., 2022. Biomineralization processes in modern calcareous tufa: possible roles of viruses, vesicles and extracellular polymeric substances (Corvino Valley–Southern Italy). Sedimentology 69 (2), 399–422.
Perri, E., Tucker, M.E., Słowakiewicz, M., Whitaker, F., Bowen, L., Perrotta, I.D., 2018. Carbonate and silicate biomineralization in a hypersaline microbial mat (Mesaieed sabkha, Qatar): roles of bacteria, extracellular polymeric substances and viruses. Sedimentology 65 (4), 1213–1245.
Petrash, D.A., Bialik, O.M., Bontognali, T.R., Vasconcelos, C., Roberts, J.A., McKenzie, J. A., Konhauser, K.O., 2017. Microbially catalyzed dolomite formation: from near-surface to burial. Earth Sci. Rev. 171, 558–582.
Préat, A., Mamet, B., Di Stefano, P., Martire, L., Kolo, K., 2011. Microbially-induced Fe and Mn oxides in condensed pelagic sediments (Middle-Upper jurassic, western sicily). Sediment. Geol. 237 (3–4), 179–188.
Qin, W., Wang, C.Y., Ma, Y.X., Shen, M.J., Li, J., Jiao, K., Franklin, R.T., Niu, L.N., 2020. Microbe-mediated extracellular and intracellular mineralization: environmental, industrial, and biotechnological applications. Adv. Mater. 32 (22), 1907833.
Reinhold, C., Kaufmann, B., 2010. Sea-level changes as controlling factor of early diagenesis: the reefal limestones of Adnet (Late Triassic, Northern Calcareous Alps, Austria). Facies 56, 231–248.
Reitner, J., 1993. Modern cryptic microbialite/metazoan facies from Lizard Island (Great Barrier Reef, Australia) formation and concepts. Facies 29, 3–39.
Reolid, M., Abad, I., 2019. Jurassic non-carbonate microbialites from the betic-rifian cordillera (Tethys western end): textures, mineralogy, and environmental reconstruction. Minerals 9 (2), 88.
Riding, R., 1991. Classification of microbial carbonates. In: Riding, R. (Ed.), Calcareous Algae and Stromatolites. Springer-Verlag, Berlin, pp. 21–51.
Riding, R., 2000. Microbial carbonates: the geological record of calcified bacterial–algal mats and biofilms. Sedimentology 47, 179–214.
Riding, R., 2002. Biofilm architecture of Phanerozoic cryptic carbonate marine veneers. Geology 30, 31–34.
Rodríguez-Martínez, M., Heim, C.M., Quéric, N.V., Reitner, J., 2011. Frutexites. In: Reitner, J., Thiel, V. (Eds.), Encyclopedia of Geobiology. Springer, Dordrecht, pp. 396–401.
Russo, F., Gautret, P., Mastandrea, A., Perri, E., 2006a. Syndepositional cements associated with nannofossils in the Marmolada Massif: evidences of microbially mediated primary marine cements?(Middle Triassic, Dolomites, Italy). Sediment. Geol. 185 (3–4), 267–275.
Russo, F., Gautret, P., Mastandrea, A., Perri, E., 2006b. Syndepositional cements associated with nannofossils in the Marmolada Massif: evidences of microbially mediated primary marine cements? (Middle Triassic, Dolomites, Italy). Sediment. Geol. 185, 267–275.
Sanfilippo, R., Rosso, A., Guido, A., Mastandrea, A., Russo, F., Riding, R., Taddei Ruggiero, E., 2015. Metazoan/microbial biostalactites from present-day submarine caves in the Mediterranean Sea. Mar. Ecol. 36 (4), 1277–1293.
Sano, H., Nakashima, K., 1997. Lowermost Triassic (Griesbachian) microbial bindstone-cementstone facies, southwest Japan. Facies 36, 1–24.
Santagati, P., Perri, E., Bernasconi, M.P., Borrelli, M., Guerrieri, S., Critelli, S., 2024. MIS 5e Sea Surface Temperature estimation; a multi-proxy approach using a marine macrofossil assemblage (Mar Piccolo, Gulf of Taranto, Southern Italy). J. Palaeogeogr. 13 (2), 327–350.
Santantonio, M., Teale, C.T., 1987. An example of the use of detrital episodes in elucidating complex basin histories: the Caloveto and Longobucco Groups of N.E. Calabria, S. Italy. In: Leggett, J.K., Zuffa, G.G. (Eds.), Marine Clastic Sedimentology. Graham & Trotman, London, pp. 62–74.
Santantonio, M., Fabbi, S., 2020. Anatomy and jurassic evolution of a hercynian basement high (Caloveto high-calabria, southern Italy). Italian Journal of Geosciences 139, 30–53.
Santantonio, M., Fabbi, S., Bigi, S., 2017. Discussion on «Geological map of the partially dolomitized Jurassic succession exposed in the central sector of the Montagna dei Fiori Anticline, Central Apennines. Italian Journal of Geosciences 136, 312–316. Italy» by Storti, G., Balsamo, F., Koopman, A., 2017.
Santantonio, M., Innamorati, G., Cipriani, A., Antonelli, M., Fabbi, S., 2024. An exceptionally well-preserved Jurassic plateau-top to marginal escarpment in the Northern Apennines (Central Italy): sedimentological, palaeontological and palaeostructural features. J. Iber. Geol. https://doi.org/10.1007/s41513-024-00243-z.
Santantonio, M., Fabbi, S., Aldega, L., 2016. Mesozoic architecture of a tract of the European–Iberian continental margin: insights from preserved submarine

palaeotopography in the Longobucco Basin (Calabria, Southern Italy). Sediment. Geol. 331, 94–113.
Shackleton, N.J., Kennett, J.P., 1975. Paleotemperature history of the Cenozoic and the initiation of Antarctic glaciation: oxygen and carbon isotope analyses in DSDP sites 277, 279, and 281. Initial Rep. Deep Sea Drill. Proj. 29, 743–755.
Stolper, D.A., Eiler, J.M., 2015. The kinetics of solid-state isotope-exchange reactions for clumped isotopes: a study of inorganic calcites and apatites from natural and experimental samples. Am. J. Sci. 315 (5), 363–411.
Taber, S., 1916. The growth of crystals under external pressure. Am. J. Sci. 246, 532–556.
Van der Kooij, B., Immenhauser, A.M., Steuber, T., Samankassou, E., Bahamonde, J.R., Merino Tomé, O., 2007. Marine red staining of a Pennsylvanian carbonate slope: environmental and oceanographic significance. J. Sediment. Res. 77, 1026–1045.
Walter, M.R., Awramik, S.M., 1979. Frutexites from stromatolites of the gunflint iron formation of Canada, and its biological affinities. Precambrian Res. 9, 23–33.
Webb, G.E., Baker, J.C., Jell, J.S., 1998. Inferred syngenetic textural evolution in holocene cryptic reefal microbialites, heron reef, great barrier reef, Australia. Geology 26, 355–358.
Young, J.R., Teale, C.T., Bown, P.R., 1986. Revision of the stratigraphy of the Longobucco Group (Liassic, Southern Italy); based on new data from nannofossils and ammonites. Eclogae Geol. Helv. 79, 117–135.
Zankl, H., 1993. The origin of high-Mg-calcite microbialites in cryptic habitats of Caribbean coral reefs-their dependence on light and turbulence. Facies 29, 55–59.
Zhao, D., Tan, X., Hu, G., Wang, L., Wang, X., Qiao, Z., Luo, S., Tang, H., 2021. Characteristics and primary mineralogy of fibrous marine dolomite cements in the end-Ediacaran Dengying Formation, South China: implications for aragonite–dolomite seas. Palaeogeogr. Palaeoclimatol. Palaeoecol. 581, 110635.